



# Gravity field recovery from geodetic altimeter missions

David T. Sandwell <sup>a,\*</sup>, Hugh Harper <sup>a</sup>, Brook Tozer <sup>a</sup>, Walter H.F. Smith <sup>b</sup>

<sup>a</sup> Institute of Geophysics and Planetary Physics, Scripps Institution of Oceanography, University of California San Diego, La Jolla, CA 92093, USA

<sup>b</sup> NOAA Laboratory for Satellite Altimetry, College Park, MD 20740, USA

Received 18 April 2019; received in revised form 3 September 2019; accepted 6 September 2019

## Abstract

Satellite radar altimetry collected during a number of geodetic missions has provided a new understanding of the topography and tectonics of the deep oceans. As altimeter performance and coverage improves, smaller structures are revealed. Here we investigate the contribution of six altimeter missions that have been placed into geodetic mapping phases for more than one year. Two types of evaluations are performed. We first compare the composite (all six altimeters) grids of east and north vertical deflection to matching grids where one altimeter has been omitted evaluate their contribution versus latitude. We then estimate the noise in each altimeter by computing the median absolute deviation of the profiles with the best composite grid. Both analyses show that SARAL/AltiKa provides the greatest contribution and ERS-1 no longer provides any significant improvement. The major limitation for recovering small scale gravity features is the sea surface roughness from ocean waves. There have been steady improvements in instrumentation and processing methods that will continue into the future with higher frequency radars and interferometric swath altimeters planned for future missions.

© 2019 COSPAR. Published by Elsevier Ltd. All rights reserved.

**Keywords:** Marine gravity; Radar altimetry; Seafloor tectonics; Ocean variability

## 1. Introduction

It has been 34 years since the Geosat altimeter began its geodetic mission (GM) to provide the first comprehensive mapping of the marine gravity field between latitudes of  $\pm 72^\circ$ . Since then there have been 5 radar altimeters having geodetic mapping phases one year or longer (Table 1). Here we assess the contribution of each geodetic mission to the recovery of the marine gravity field. Gravity field recovery depends on three factors: (1) altimeter range precision which is related to the characteristics of the radar (Raney and Phalippou, 2011); (2) spatial coverage which is related to mission duration; and (3) track orientation which is related to orbital inclination and latitude. Over the years, there have been many publications on the incremental improvements in gravity accuracy and resolution; the

current retracking and gravity construction methods are now quite stable (Haxby and Weissel, 1986; Hwang, 1998; Fu and Cazenave, 2001; Deng and Featherstone, 2006; Andersen et al., 2010; Sandwell and Smith, 2009; Zhang and Sandwell, 2017).

Since 2010, the main improvements have been related to having more data available from CryoSat-2, Jason-1, Jason-2 and SARAL/AltiKa (abbreviated AltiKa) in their geodetic phases. These altimeters also have improved range precision with respect to ERS-1 and Geosat. Moreover, they span a range of orbital inclination coverage and three of these altimeters are still collecting data. The main purpose of this paper is to rank the GM altimeters in terms of their contribution to the marine gravity field today (our latest version number V28), assess whether the older data are still providing gravity information, provide an updated marine gravity anomaly map including uncertainty, and finally present a new map of ocean mesoscale variability that highlights features at 25 km spatial

\* Corresponding author.

E-mail address: [dsandwell@ucsd.edu](mailto:dsandwell@ucsd.edu) (D.T. Sandwell).

Table 1

Summary of geodetic altimeter data used in the latest gravity grid (V28).

Altimeter	Start of GM phase	Duration (mo.)	Latitude coverage	Noise@20 Hz and 2 m SWH (mm)	Reference
Geosat	APR 1985 <sup>#</sup>	18	±72°	57.0	Sandwell and Smith, 2009
ERS-1	APR 1994	12	±81°	61.8	Sandwell and Smith, 2009
Jason-1/2	APR 2012/AUG 2017	14/12+	±66°	46.4/44.0	Garcia et al., 2014, Appendix A
CryoSat-2 LRM/SAR	JUN 2010	96+	±88°	42.7/49.7	Garcia et al., 2014
SARAL/AltiKa	JUN 2016	32+	±81°	28.9 <sup>+</sup>	Zhang and Sandwell, 2017

In addition to the GM coverage provided in the table, we used 2520 days of 35-day repeat Envisat data, 3700 days of 10-day repeat Jason-1 data, 150 days of 10-day repeat Jason-2 data and 1225 days of 35-day repeat SARAL/AltiKa data.

<sup>#</sup> Geosat/GM data were declassified in June 1995 after ERS-1 completed its GM.

<sup>+</sup> SARAL/AltiKa noise at 40 Hz.

resolution. This new variability can only be recovered with the dense spatial coverage provided by the geodetic phases.

## 2. Current spatial coverage and new gravity model

The altimeter data used for this study are the 20 or 40 Hz waveform data freely available from NOAA, CNES, ISRO, ESA, and NASA as of March 15, 2019. All the raw waveform data were retracked using the two-pass method described in Garcia et al., 2014 and Zhang and Sandwell (2017). The results are comparable to other two-pass retracking approaches (e.g., Andersen et al., 2010; Amarouche et al., 2014) where the range precision is improved by a factor of 1.5–1.6 with respect to the standard Geophysical Data Records (GDR). Appendix A provides new research results on the retracking of the 20 Hz waveform data from Jason-2.

The ground tracks over a region around Hawaii are shown in Fig. 1 for all the GM data described in Table 1. The along-track sea surface slope is shown in these plots. The largest amplitude slopes are associated with the gravity field of Hawaii. Smaller amplitude slopes are associated with fracture zones and seamounts. Track density mainly depends on mission duration. CryoSat-2 has the highest track density owing to its 96 months of data coverage.

We used these data in a remove/grid/restore approach to construct a variety of gravity products that are more fully described in Zhang et al. (2017). That study includes a complete description of the along-track filters and editing that were applied to the slope profiles. Residual along-track slopes (w.r.t. EGM2008; Pavlis et al., 2012) and uncertainties based on significant wave height were combined using a least squares biharmonic gridding approach (Wessel and Bercovici, 1998; Sandwell and Smith, 2009) to form grids of north and east deflection of the vertical. These were transformed using Laplace's equation to produce grids of gravity anomaly and uncertainty (Fig. 1g,h) as well as vertical gravity gradient (VGG) (Fig. 1f). The final 2-D filter applied to the gravity products is depth dependent where shallower areas (<2 km) have a shorter wavelength filter (12 km wavelength) and deeper areas (>6 km) longer wavelength filter (17 km wavelength). The

filter wavelength increases linearly with depth between these limits). This depth-dependent filter is used because the short wavelength gravity signal is naturally attenuated by upward continuation.

## 3. Altimeter ranking

The contribution of each altimeter to gravity field recovery is determined using two approaches. In the first approach we compare north and east grids of vertical deflection derived in a variety of data exclusion scenarios. We presume that the most accurate vertical deflection grids are produced when all the GM altimeter data are included. Note this new gravity compilation (V28) also includes 7 years of Envisat altimeter data from its 35-day repeat phase as well as a few months of Envisat data from its “drifting” orbital phase. We then re-compute the vertical deflection grids where one or more altimeter data sets are excluded. The resulting differences are calculated in latitude bands to highlight the differences that depend on track orientation. In the second approach we calculate the median absolute deviation of the along-track slope data with respect to the full (V28) slope grids and presume the deviations are mostly related to the noise in the altimeter profiles. From this we compute the rms in 20° by 20° areas and use this to rank the altimeters.

### 3.1. Improvement V28 vs. V18 and V23

The first analysis compares the differences between the present (best) vertical deflection grids (V28) and two previously published versions. The V18 vertical deflections were based on only retracked ERS-1 and Geosat/GM data (Sandwell and Smith, 2009) while V23 also included 42 months of retracked CryoSat-2 data and 14 months of retracked Jason-1/GM data, and 2 years of Envisat 35-day repeat data (Sandwell et al., 2014). The results are shown in Fig. 2. The upper plot shows the median absolute deviation between the north and east grids of V28 and V18 averaged over bands of constant latitude. The largest differences occur at latitudes greater than 72° degrees where the new high latitude data from CryoSat-2 and SARAL/

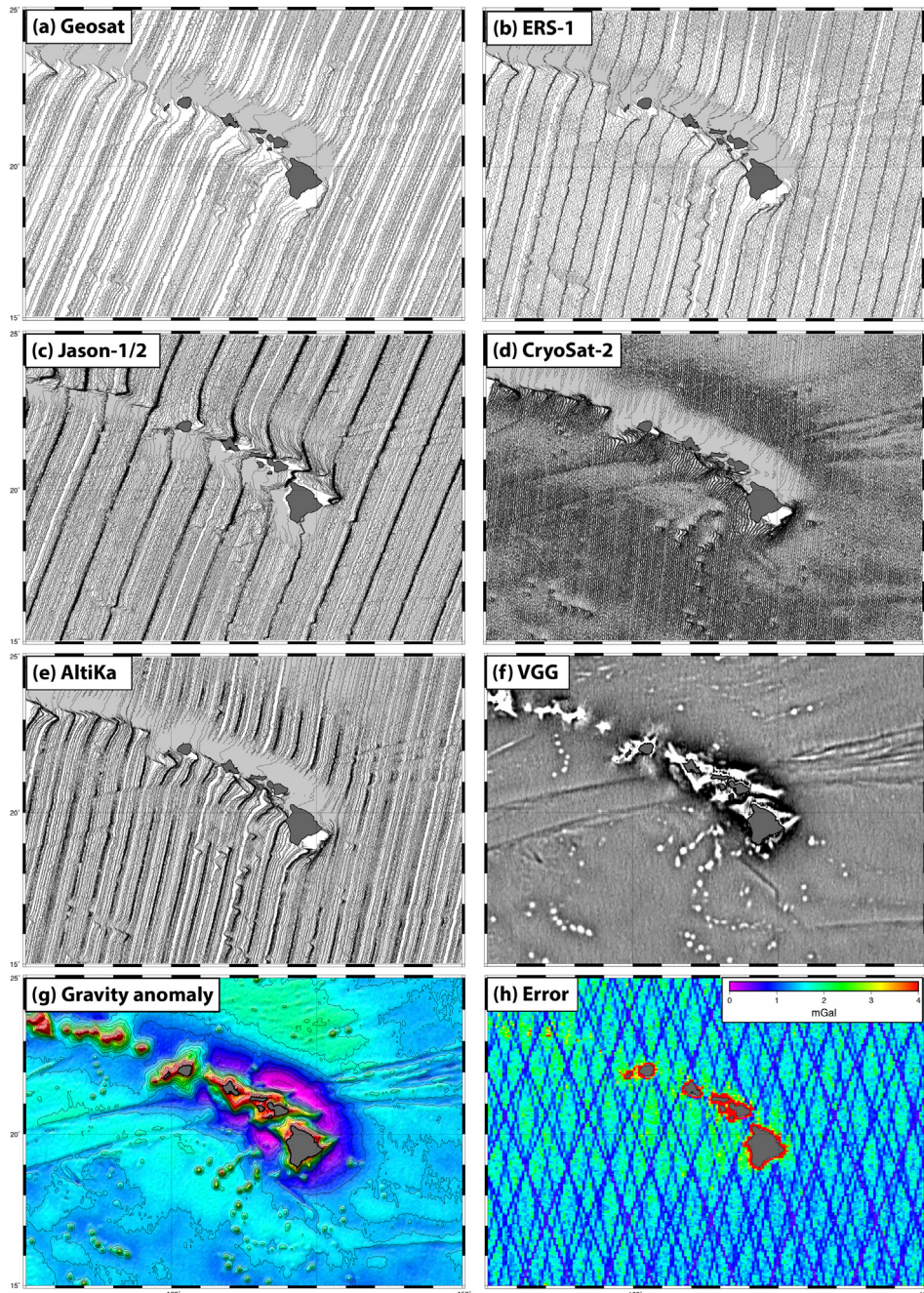


Fig. 1. . Along track sea surface slopes from (a) Geosat, (b) ERS-1, (c) Jason-1/2, (d) CryoSat-2, and (e) AltiKa. The vertical gravity gradient, gravity anomaly (contour interval 20 mGal), and gravity uncertainty are provided in (f), (g), and (h), respectively.

AltiKa provide major improvements. At lower latitudes the improvement in the east component is typically  $2.5 \mu\text{rad}$  while the improvement for the north component is somewhat smaller at  $\sim 2 \mu\text{rad}$ . The lower plot shows the same as above but for the V28 and V23 models. In this case the differences are smaller reflecting a smaller improvement of V28 with respect to V23. Nevertheless, the differences are mostly greater than  $1 \mu\text{rad}$  and are most important for the east component. The main differences between

V28 and V23 are due to including new data from SARAL/AltiKa, Jason-2, and CryoSat-2.

### 3.2. Importance of each altimeter

In order to better understand the contribution of each altimeter data set we performed the same type of comparison but systematically removed data contributions from SARAL/AltiKa, CryoSat-2, Jason-1/2, Geosat, and

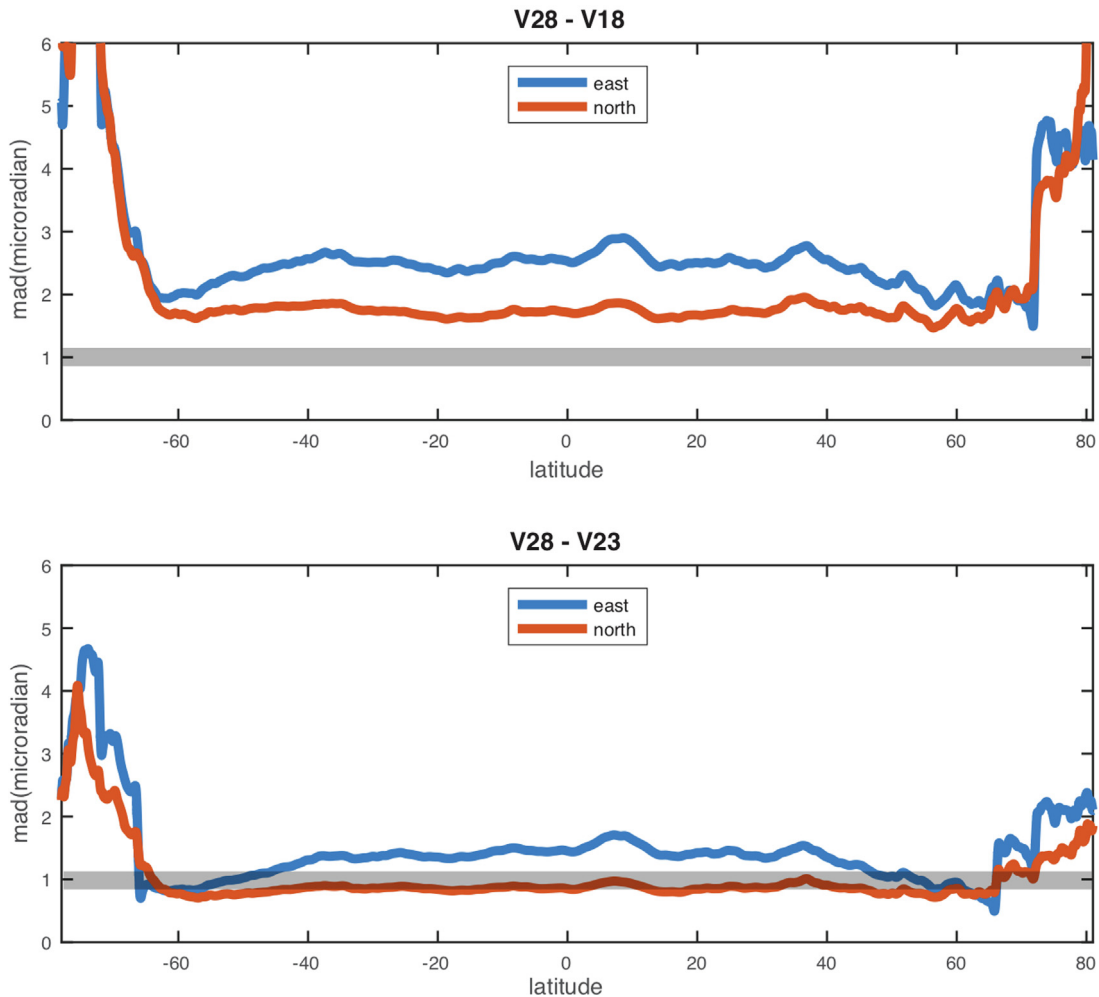


Fig. 2. Median absolute difference in microradian between the V28 gravity model and previously published model having less GM data. A larger difference is a greater improvement. All models are filtered with a 0.5 gain at 16 km full wavelength. The differences are computed in latitude bands and plotted versus latitude which reveals the differences in contribution in the east and north components due to the differing track orientations of the altimeters.

ERS-1, respectively. Note the results are plotted in Fig. 3 at differing vertical scales although for each plot the horizontal gray line marks the 1  $\mu$ rads improvement level. From this analysis it is evident that SARAL/AltiKa provides the most improvement at high latitudes as well as the most improvement in the east component at low latitudes. CryoSat-2 provides some improvement at all latitudes. Jason-1/2 provides a significant improvement in the east component and a large improvement at its turning latitudes of  $\pm 66^\circ$ . All three of these newer altimeters are providing a significant contribution and all three are still collecting data so the gravity accuracy will continue to improve.

The improvements from the older Geosat and ERS-1 altimeters is significantly less than 1  $\mu$ rads over most latitudes although Geosat does provide a significant improvement between latitudes of  $66^\circ$  and  $72^\circ$ . The improvement from ERS-1 is uniformly small and it also has the worst range precision (Table 1). Therefore, we have not included

these data in the final V28 gravity products because they may actually add noise to the composite model.

### 3.3. Global noise maps for each altimeter

The second approach for assessing the contribution of each altimeter is to calculate the median absolute deviation of the along-track slope data with respect to the full (V28) slope grids and presume that the deviations are mostly related to the noise in the altimeter profiles (Fig. 4). For all altimeters the largest differences occur in the high latitude regions where sea ice is prevalent as well as areas of high mesoscale variability. The background noise level is due mainly to ocean waves. We compute the rms in two,  $20^\circ$  by  $20^\circ$  areas and use this to rank the altimeters (Table 2). The two test areas in the South Atlantic and North Pacific have relatively low mesoscale variability to measure the background noise. In both cases, SARAL/

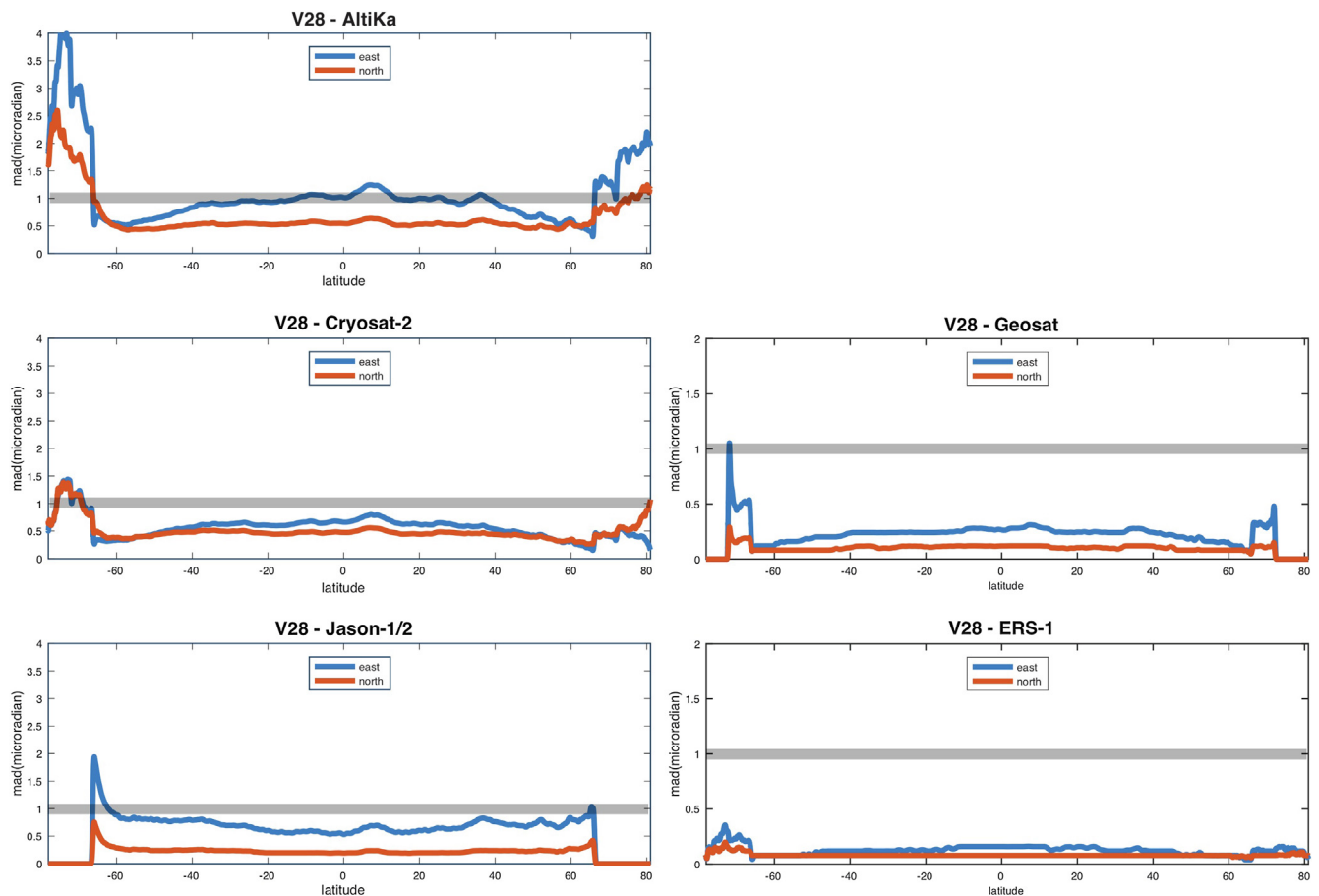


Fig. 3. Median absolute difference in microradian between the V28 gravity model and models generated with one data set omitted. A larger difference is a greater improvement. All models are filtered with a 0.5 gain at 16 km full wavelength. We treat Jason-1 and 2 as a single contribution since they have similar noise characteristics. SARAL/AltiKa provides the largest contribution especially in the east component at low latitudes. CryoSat-2 and Jason-1/2 provide significant contributions. Geosat and ERS-1 provide minor contributions.

AltiKa has, by far, the lowest noise followed by CryoSat-2, Jason-1/2, Geosat, and finally ERS-1. The noise level of ERS-1 is 2 times higher than SARAL/AltiKa thus providing further justification for not using these data in the final V28 grid. Jason-1/2 and Geosat have similar noise levels and the noise level CryoSat-2 is between SARAL/AltiKa and Jason-1/2. Given that CryoSat-2 has 3 times more data than SARAL/AltiKa, it is the most important altimeter for averaging out the mesoscale variability. Based on this noise analysis, SARAL/AltiKa is the clear winner.

#### 4. Gravity accuracy and spatial resolution

##### 4.1. Gravity assessment in Gulf of Mexico

The above analyses only provide a measure of the relative importance of each altimeter. To get a measure of the absolute accuracy, we compare the V28 gravity field, developed from the east and north grids with a dense and highly precise (~0.5 mGal) gravity grid in the Gulf of Mexico (Fig. 5). The point-wise rms difference between the V28

model filtered at 12 km wavelength and the EDCON-PRJ gravity data is 1.33 mGal suggesting the V28 gravity has an rms error of 1.23 mGal. The older models V23 and V18 has rms differences of 1.52 and 2.05 mGal, respectively. A cross spectral coherence analysis (Fig. 5) shows the improvements in coherence from the V18 model (0.25 coherence at 22 km wavelength) based only on Geosat and ERS-1 to the latest model V28 (0.25 coherence at ~12 km wavelength) which includes all the newer data. Indeed, the final 2-D smoothing filter applied to the gravity grid has 0.5 gain at 12 km at this ocean depth so the resolution is approaching the final filter wavelength and we may need to apply a shorter wavelength filter for future versions.

##### 4.2. Global gravity uncertainty

The estimated accuracy of the V28 gravity in the Gulf of Mexico enables us to develop a global uncertainty map (Fig. 6). This map is constructed by taking a block median average (5 min longitude by 3 min latitude) of the deviations of the along-track slopes from all the altimeters

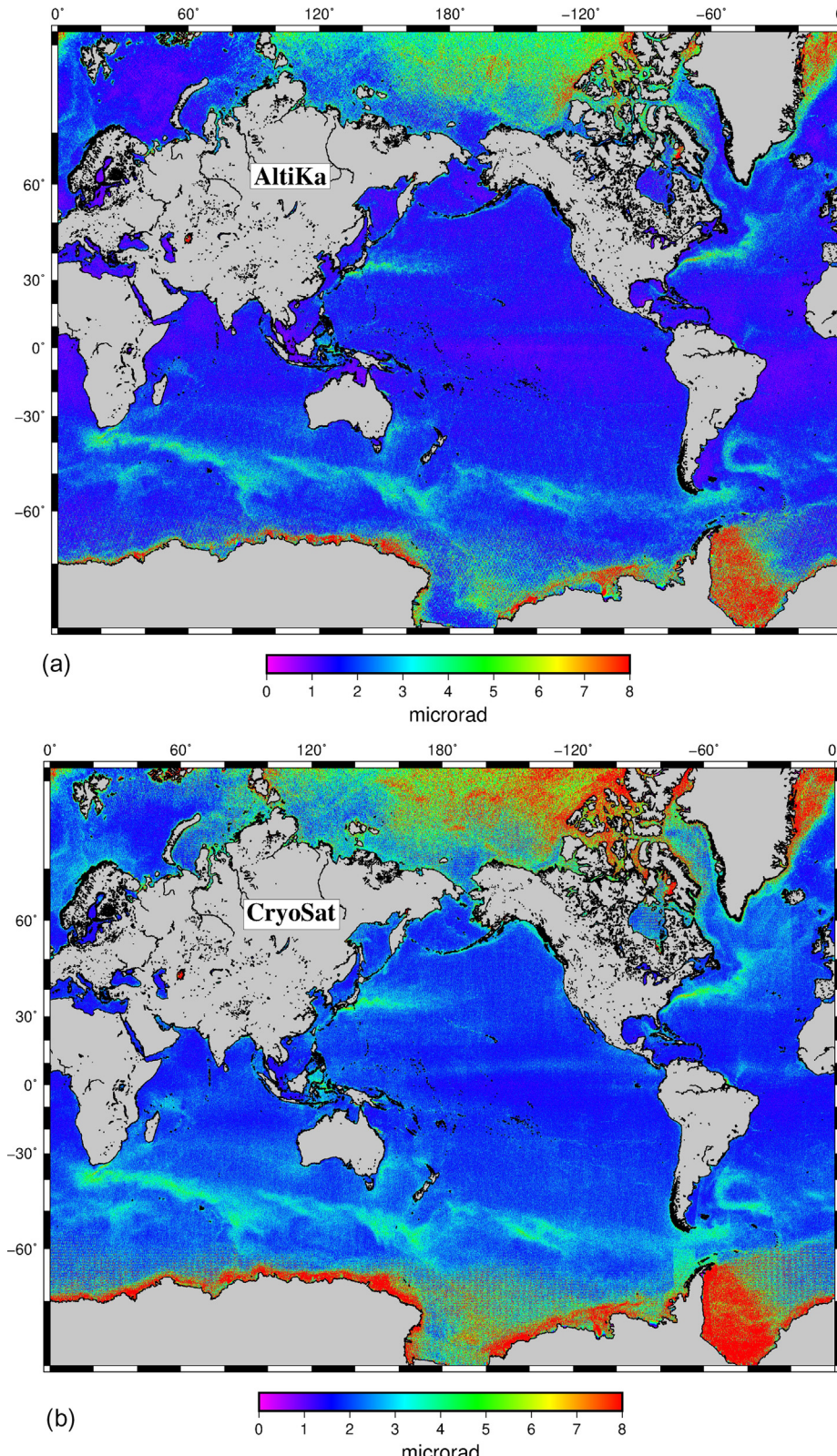


Fig. 4. Median absolute deviation of along-track slope of each altimeter with respect to the V28 model. The differences are filtered with a 0.5 gain at 18 km wavelength. For all altimeters the largest differences occur in the high latitude regions where sea ice is prevalent as well as areas of high mesoscale variability. The background noise level reflect altimeter noise that is amplified in areas of high wave height.

except for ERS-1 and dividing that by the square root of the number of observations in each cell. The cell size was selected to combine data from several satellites while not smoothing too much over the higher accuracy areas corresponding to repeat tracks. The overall map was calibrated using a scaling factor that makes the median deviation in the Alaminos Canyon area equal to the 1.33 mGal error estimate for that area (Fig. 5). Note that spatially, the error estimate is highly non-uniform (Fig. 1h and Fig. 6). Of course, the error is larger in regions of sea ice as well as higher mesoscale ocean variability. There are lines of low error that follow the tracklines of the repeat-track altimetry

data used in the construction of the grid. These are from 6.9 years of Envisat, 3.4 years of SARAL/AltiKa prior to the geodetic phase and 10.1 years of Jason-1 prior to its geodetic phase. There is very low error at the turning latitudes of Jason-1/2 (i.e.  $\pm 66^\circ$ ) and Geosat (i.e.,  $\pm 72^\circ$ ).

## 5. Oceanographic signals

Finally, we have processed the along-track slope variations to highlight oceanographic signals having wavelengths greater than 25 km (Fig. 7). Mesoscale variability maps are usually only based on repeat-track coverage

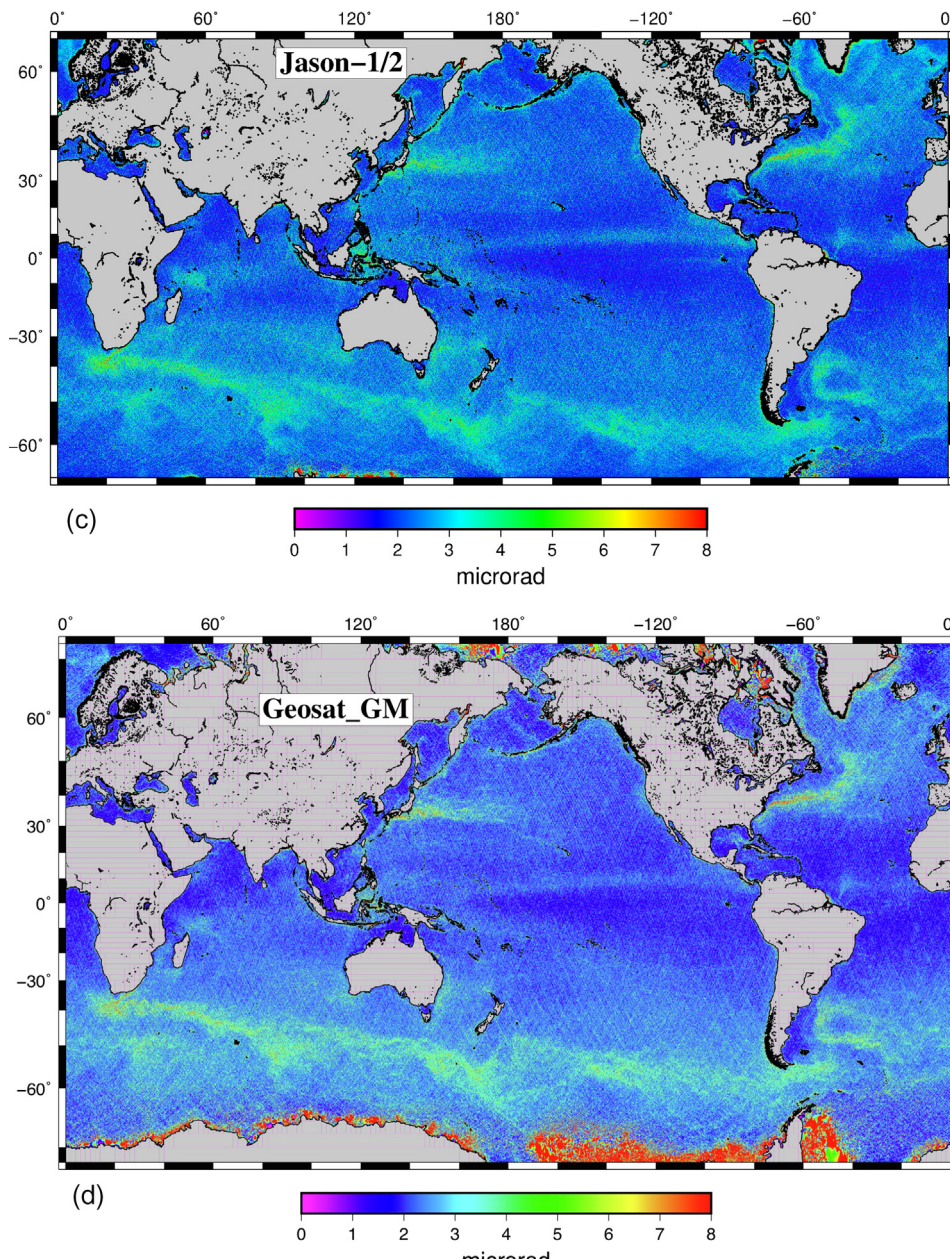


Fig 4. (continued)

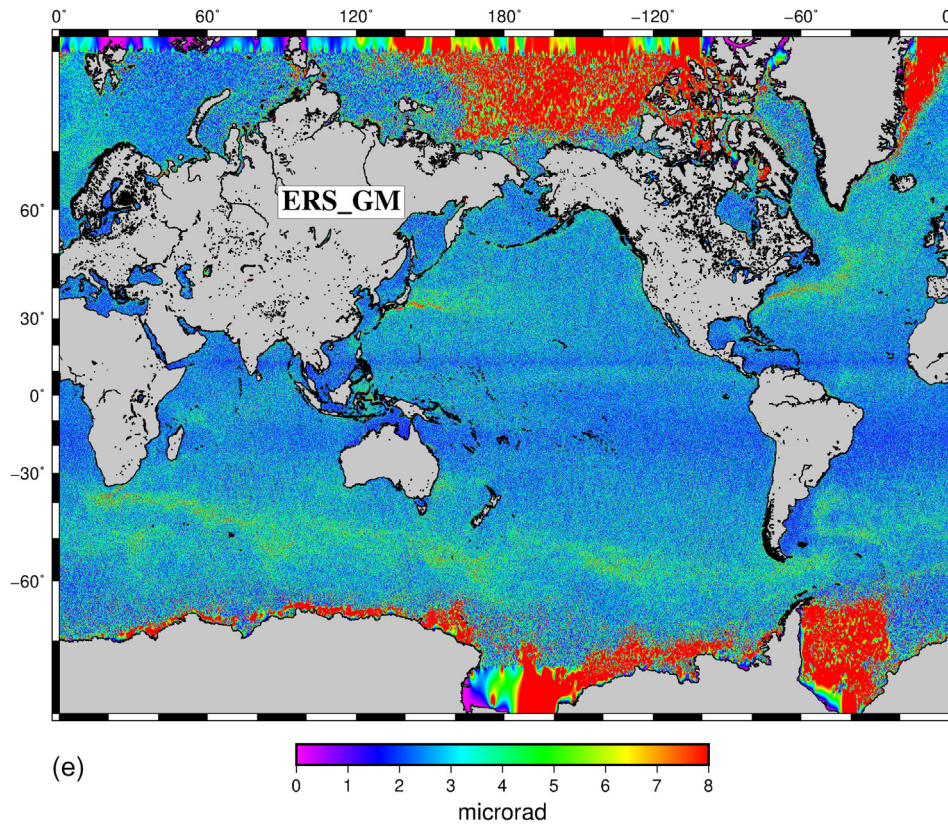


Fig 4. (continued)

Table 2

Along-track slope noise.

	Noise (microradian) $-20 < \text{lon} < 0; -20 < \text{lat} < 0$	Noise (microradian) $180 < \text{lon} < 200; 30 < \text{lat} < 50$
SARAL/AltiKa	1.16	1.55
CryoSat-2	1.56	1.98
Jason-1/2	1.80	2.33
Geosat	1.83	2.32
ERS-1	2.30	2.98

Difference between along-track slope and deflection of the vertical.

V28 low-pass filtered at 18 km wavelength.

which does not recover spatial scales less than about 100 km so this map reveals new small-scale features. The 25 km low-pass filter was selected to suppress the altimeter noise related to wave height and enhance signals due to balanced and unbalanced motions (Qiu et al., 2018). The most prominent regions of high slope variability are associated with the Kuroshio, Gulf Stream, and Antarctic Circumpolar Currents as well as other western boundary currents. Note the lack of slope variability in regions where the ocean depth is less than 1 km. Moreover, the mid ocean spreading ridges having depths less than 3 km appear as barriers to slope variability.

## 6. Outlook and conclusions

This analysis highlights the importance of each of the altimeters that have had geodetic mapping phases lasting more than 12 months. Originally, Geosat and ERS-1 were the most important altimeters for recovery of the marine gravity field (e.g., Andersen and Knudsen, 1998) with a minor improvement from 2-pass retracking (Sandwell and Smith, 2009). The launch of CryoSat-2 in 2010 provides a much lower noise data source that extends to high latitudes of 88°. CryoSat-2 has a quasi-repeat cycle of 369 days but, in fact, the tracks do not repeat exactly so the 8 years of

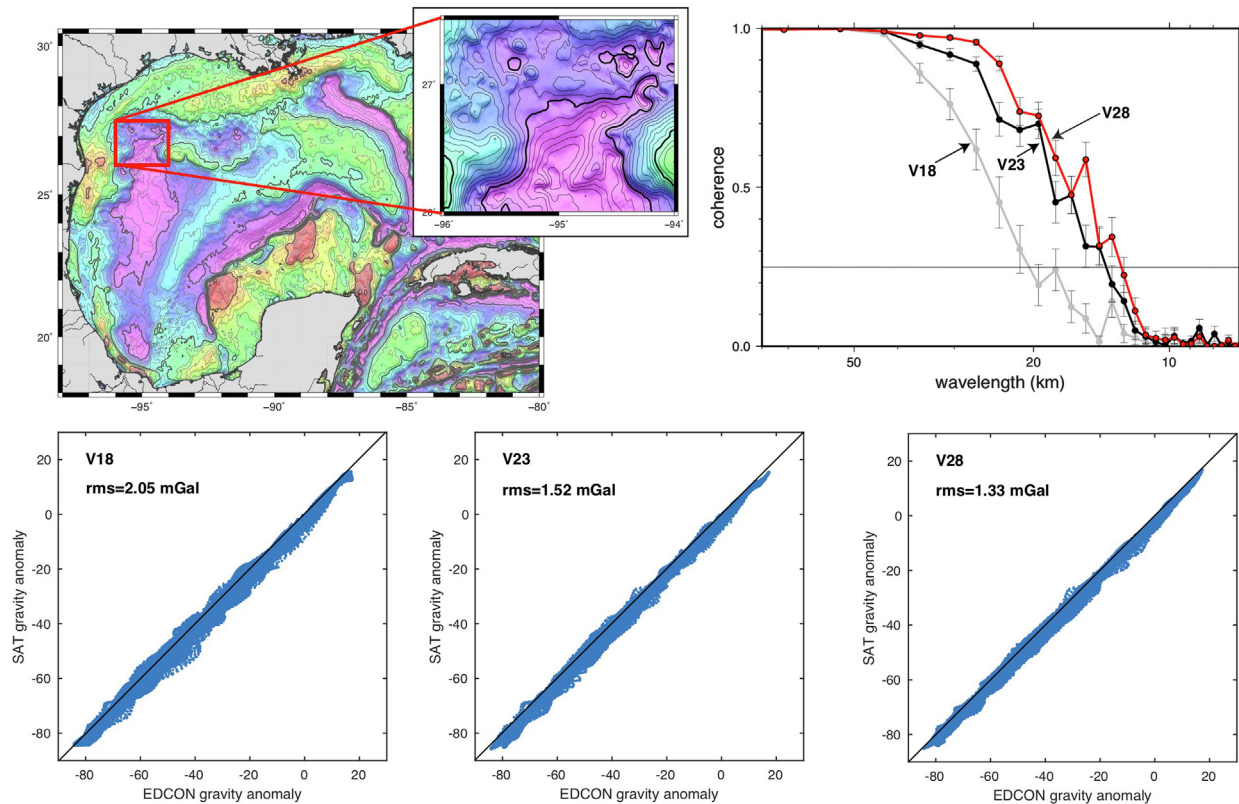


Fig. 5. Comparison of the new V28 gravity anomaly model with a higher accuracy gravity grid in the Alaminos Canyon, Gulf of Mexico (EDCON-PRJ). (upper) The coherence is close to 1 at wavelengths greater than 30 km and less than 0.25 at wavelengths  $< 12$  km. (lower) The rms deviation between the satellite gravity and the EDCON data improves from 2.05 mGal for V18 to 1.52 mGal for V23 to 1.33 mGal for V28.

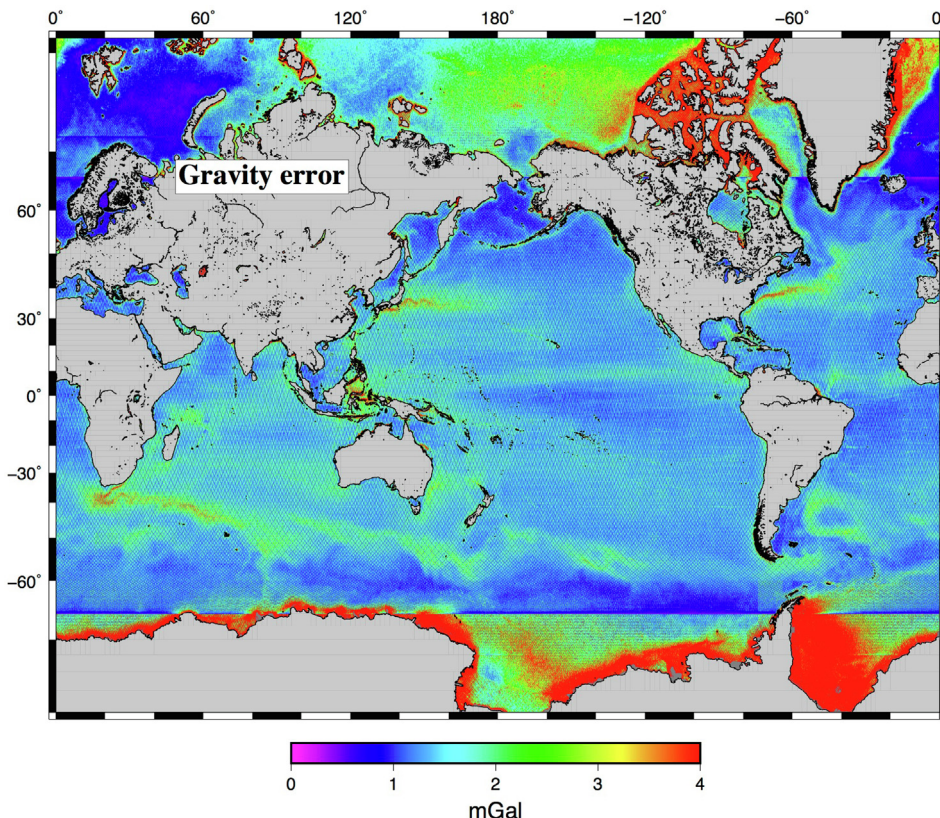


Fig. 6. Map of gravity anomaly error based on deviations of along-track slope from all altimeters divided by the square root of the number of points in the 5 min by 3 min averaging cell. The overall scale of the grid was calibrated using the rms deviation from the EDCON-PRJ grid in the Gulf of Mexico.

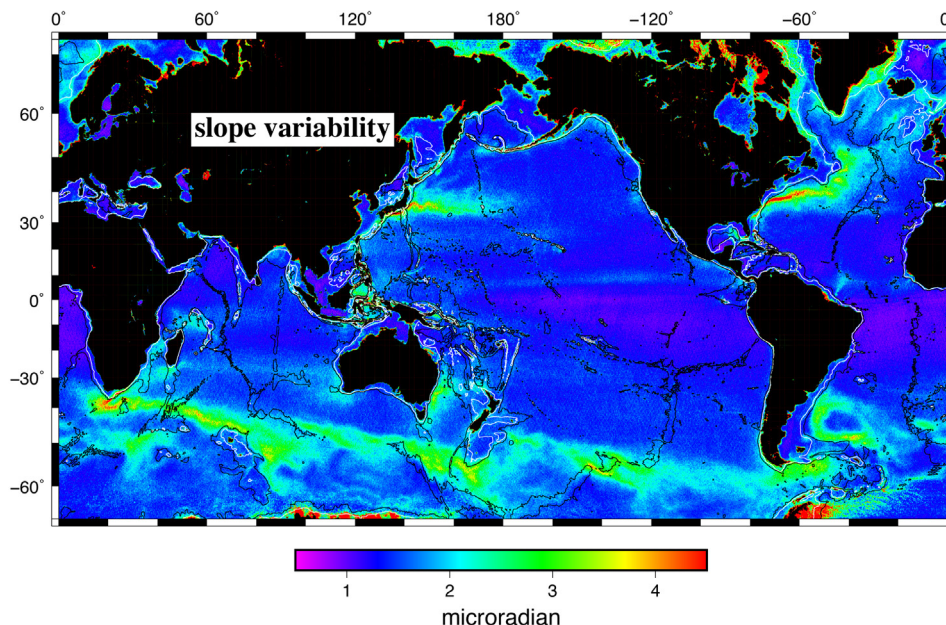


Fig. 7. Sea surface slope variability derived from the difference between along track slope and the long-term average slope from the east and north deflection of the vertical grids. The 1 km and 3 km depth contours are the white and black, respectively.

data from CryoSat-2 resulted in a tremendous improvement in marine gravity recovery especially in the Arctic basin (Andersen et al., 2014; Jain et al., 2015). Both Jason-1 and Jason-2 were placed in geodetic mapping phases as extension of life missions (Dibarbour and Morrow, 2016) and they have provided major increases in the gravity recovery especially the east-west component at low latitudes. Finally, SARAL/AltiKa with its high range precision (Zhang and Sandwell, 2017) is rapidly becoming the most important altimeter for gravity field recovery. The current 32 months of data have noise levels that are at least 1.3 times better than CryoSat-2. Overall these 32 months of SARAL/AltiKa data are more important than the 96 months of CryoSat-2 data. If this mission continues for another few years, the accuracy of the gravity field will become much closer to our 1 mGal objective (Sandwell et al., 2006). Moreover, many repeat measurements are needed to reduce the oceanographic signals that contaminate the mean sea surface. The combination of repeated measurements from Envisat, Jason-1/2, CryoSat-2, and now SARAL/AltiKa will provide a baseline mean sea surface that is needed for the upcoming SWOT experiment in order to isolate the oceanographic signals early in the mission.

## Acknowledgements

The authors thank ESA, NASA, ISRO and CNES for the open policy and access to the raw waveform data on all the altimeter datasets. We thank the two reviewers and the guest editor for their careful evaluations. This work was supported by the NASA SWOT program

(NNX16AH64G) and the Office of Naval Research (N00014-17-1-2866). The Generic Mapping Tools (Wessel et al., 2013) were used extensively in data analysis and to generate figures. The manuscript contents are solely the findings of the authors and do not constitute a statement of policy, decision, or position on behalf of NOAA or the U.S. Government.

## Appendix A. Retracking Jason-2 data

Here we follow the approach of Garcia et al. (2014) and Zhang et al. (2018) to develop the retracking parameters and assess the range precision of Jason-2 altimeter data. The raw waveform data, in sensor geophysical data records (SGDR) format, are available from Aviso and NOAA at [ftp://nодc.noaa.gov/nодc/data/jason2-xgdr/gdr/s\\_gdr](ftp://nодc.noaa.gov/nодc/data/jason2-xgdr/gdr/s_gdr). We use a simplified Brown (1977) parameterization and stress we are only interested in the sea surface slope along the satellite track. The waveform model  $M$  is

$$M(t) = \frac{A}{2} \left[ 1 + \text{erf} \left( \frac{t - t_o}{\sqrt{2}\sigma} \right) \right] e^{-\alpha(t-t_o)} \quad (0.1)$$

where  $A$  is the amplitude of the waveform,  $t_o$  is the arrival time,  $\sigma$  is the rise time, and  $\alpha$  is the trailing edge decay parameter. Note that  $\sigma^2 = \sigma_p^2 + \sigma_h^2$  where  $\sigma_p$  is the effective resolution of the radar pulse and  $\sigma_h$  is ¼ of the significant wave height (SWH). The trailing edge decay parameter is related to the beam width of the antenna pattern projected on the ocean surface as well as possible off-nadir pointing. The pointing of Jason-2 was well controlled so we assume that  $\alpha$  is a constant for the entire mission. To estimate this

constant  $\alpha$  we started with several long passes across the Atlantic and Indian oceans and retracked them using a least squares approach (Garcia et al., 2014) to solve for the parameters  $(A, t_o, \sigma)$ . We swept through a range of  $\alpha$  until the rms misfit of all the waveforms in the set was minimized. The corresponding  $\alpha$  was  $0.0065$  gates $^{-1}$  which is similar to the value for Jason-1 of  $0.0058$  gates $^{-1}$  (Zhang

et al., 2018). We used this fixed value for retracking all the Jason-2 data.

Retracking was done in 4 steps: (1) The first step is to use a threshold retracker to roughly estimate the arrival time parameter  $t_o$ . This estimate is used as a starting point for the three-parameter inversion  $(A, t_o, \sigma)$ . (2) The inversion is performed on three adjacent 20-Hz waveforms

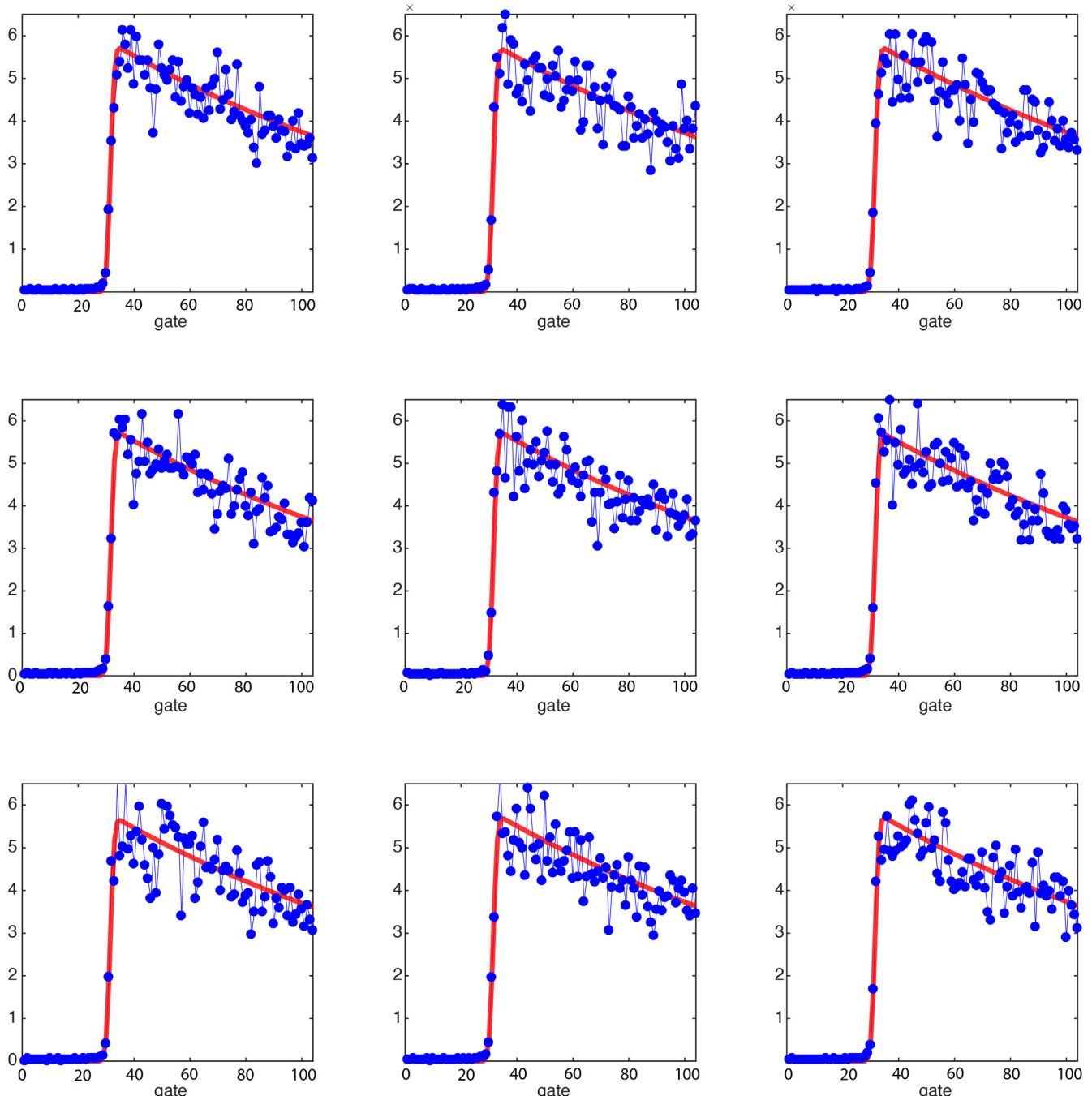


Fig. A1. A set of adjacent retracked waveforms. The blue circles are the data, the red line the two-parameter retracked waveform. The waveforms shown here have a typical rise time with SWH of around 2 m.

where the outer two waveforms are given a weight of one half the inner waveform; this approach was found to be optimal in previous similar studies (e.g. Garcia et al., 2014). (2) After this three-parameter retracking, the rise time parameter (i.e.,  $\sigma$ , or SWH) is smoothed along track with a low pass filter with a 0.5 gain at a wavelength of 45 km. (4) The rise time was set to this smoothed value in a second inversion which only solved for the two remaining parameters ( $A, t_o$ ). Forcing the SWH to a smoothed and prescribed value, serves to partially decouple the correlated errors of rise time and arrival time (Sandwell and Smith, 2005; Amarouche et al., 2014; Zaron and DeCarvalho, 2016). Example fits to some Jason-2 waveforms are shown in Fig. A1. All Ku-band altimeters have a gate spacing of 468 mm so the retracker must be able to recover 1/10 of this gate spacing to achieve the 44 mm precision noted in Table 1. Note that SARAL/AltiKa has a higher bandwidth chirp resulting in a smaller gate spacing of 31 mm. This narrower pulse range resolution combined with a 2 times higher PRF is partly responsible for the 2 times higher precision (Raney and Phalippou, 2011). The use of Ka, rather than Ku, band radar also causes the waveform trailing edge to be beam-limited,

which also contributes to the higher precision (Smith, 2015).

For the 20-Hz retracked data, we compute a noise value as the median absolute deviation from the 1-Hz median sea-surface height value. Fig. A2 shows the noise as a function of significant wave height (SWH) for the three-parameter and two-parameter retracked data. For a typical SWH value of two meters, the median noise is improved by a factor of 1.66, which is comparable to values from other altimeters (Garcia et al., 2014).

It is also helpful to look at the retracked sea-surface height in the frequency domain by computing power spectra for a satellite track, a measure of the variance as a function of wavelength. Fig. A3a shows the power spectra for retracked heights over a single track in the Indian Ocean. At longer wavelengths, the power is the same for the three- and two-parameter retracked data. This follows directly from the low-pass filter applied between the two parameter estimation steps. Between wavelengths of 90 and 5 km, the power between the two height estimates deviates; this is illustrated in Fig. A3b which shows the power spectrum of the height difference. The spectral hump shows where the most improvement is made in the two-pass

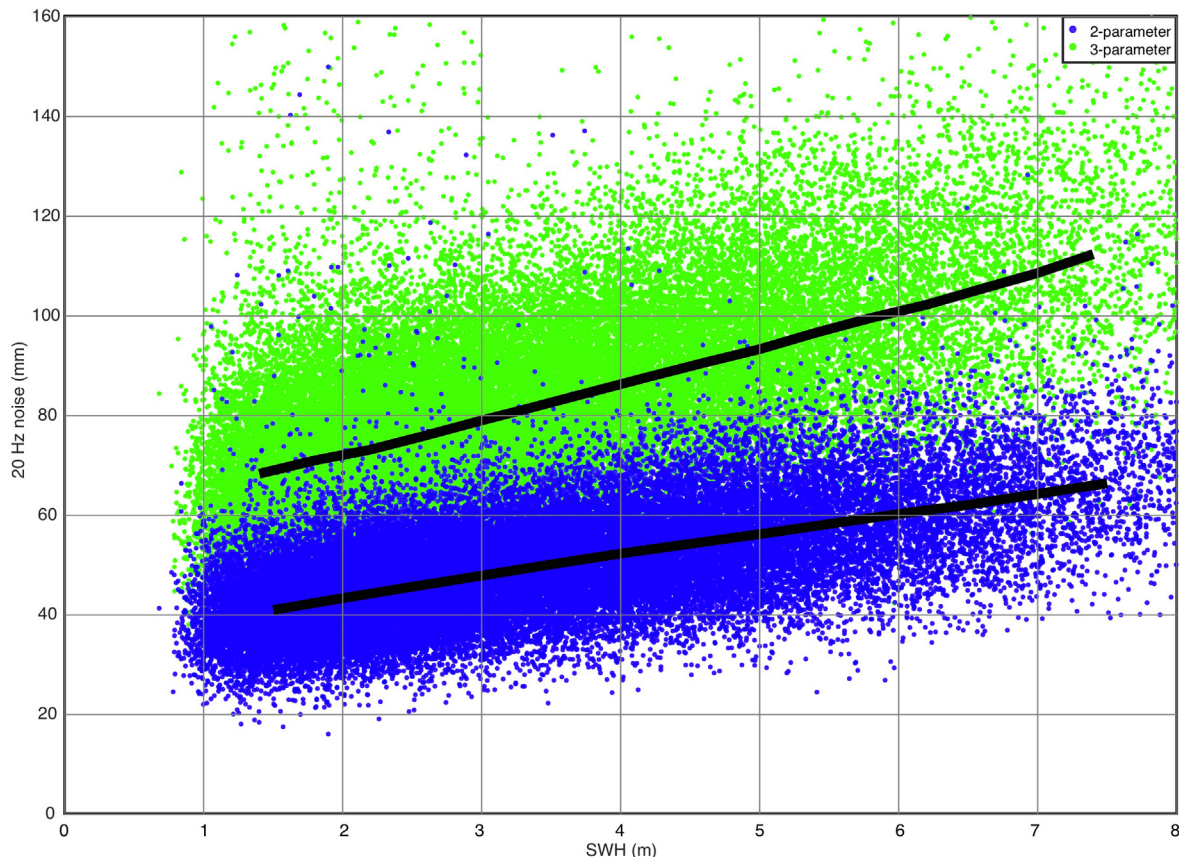


Fig. A2. The 1 Hz median noise of the 20 Hz retracked data as a function of significant wave height in a study area in the north Atlantic. 2 m is a common SWH; 6 m is considered an extreme. The one-meter-binned median noise is shown by the lines. The two-parameter retracked noise improves on the three-parameter retracked noise by a factor of 1.66.

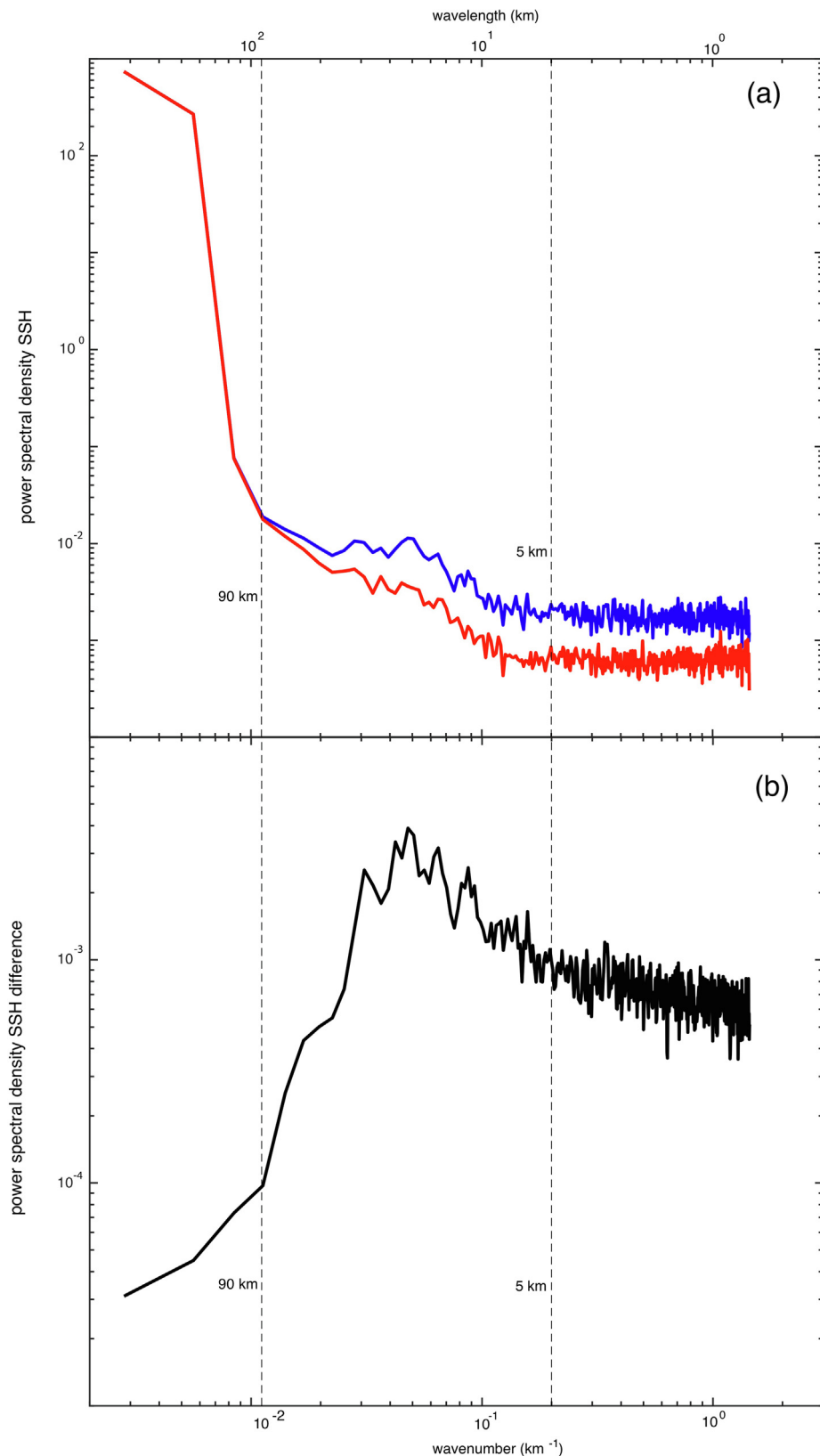


Fig. A3. (a) Power spectral density for retracted sea surface height for a long pass in the southeast Indian Ocean. Vertical lines correspond to wavelengths of 90 and 5 km. The three-parameter (blue) and two-parameter (red) estimated power spectra begin to deviate at wavelengths less than 90 km—this is a product of the low-pass filter between the retracking steps. Less than 5 km wavelengths, both spectra are essentially white. (b) Power spectral density difference between 2- and 3-parameter retracked height. The “hump” between wavelengths of 90 and 5 km highlights the noise reduction due to the two-step retracking. (For interpretation of the references to colour in this figure legend, the reader is referred to the web version of this article.)

retracking process. At wavelengths shorter than 5 km, the spectra are white.

## References

- Andersen, O.B., Knudsen, P., 1998. Global marine gravity field from the ERS-1 and Geosat geodetic mission altimetry. *J. Geophys. Res.: Oceans* 103 (C4), 8129–8137.
- Andersen, O.B., Knudsen, P., Berry, P.A., 2010. The DNSC08GRA global marine gravity field from double retracked satellite altimetry. *J. Geod.* 84 (3), 191–199.
- Andersen, O.B., Knudsen, P., Kenyon, S., Holmes, S., 2014, June. Global and arctic marine gravity field from recent satellite altimetry (DTU13). In: Presented at the 76th EAGE Conference and Exhibition 2014, 10.3997/2214-6409.20140897.
- Amarouche, L., Zawadzki, L., Vernier, A., Dibarboore, G., Labroue, S., Raynal, M., Poisson, J., 2014. Reduction of the sea surface height spectral hump using a new retracker decorrelating ocean estimated parameters (DCORE). In: Presented at the Ocean Surface Topography Science Team meeting “New frontiers of altimetry” was held on October 28–31, 2014 at Lake Constance, Germany.
- Brown, G., 1977. The average impulse response of a rough surface and its applications. *IEEE Trans. Antennas Propag.* 25 (1), 67–74.
- Deng, X., Featherstone, W.E., 2006. A coastal retracking system for satellite radar altimeter waveforms: Application to ERS-2 around Australia. *J. Geophys. Res. Oceans* 111, C06012.
- Dibarboore, G., Morrow, R., 2016. Value of the Jason-1 geodetic phase to study rapid oceanic changes and importance for defining a Jason-2 geodetic orbit. *J. Atmos. Oceanic Technol.* 33 (9), 1913–1930.
- Fu, L.-L., Cazenave, A., 2001. Satellite altimetry and earth sciences: a hand-book of techniques and applications. Academic Press, San Diego, ISBN-10: 0122695453.
- Garcia, E.S., Sandwell, D.T., Smith, W.H., 2014. Retracking cryosat-2, envisat and jason-1 radar altimetry waveforms for improved gravity field recovery. *Geophys. J. Int.* 196 (3), 1402–1422.
- Haxby, W.F., Weissel, J.K., 1986. Evidence for small-scale mantle convection from Seasat altimeter data. *J. Geophys. Res. Solid Earth* 91 (B3), 3507–3520.
- Hwang, C., Kao, E.C., Parsons, B., 1998. Global derivation of marine gravity anomalies from Seasat, Geosat, ERS-1 and TOPEX/POSEIDON altimeter data. *Geophys. J. Int.* 134 (2), 449–459.
- Jain, M., Andersen, O.B., Dall, J., Stenseng, L., 2015. Sea surface height determination in the Arctic using Cryosat-2 SAR data from primary peak empirical retrackers. *Adv. Space Res.* 55 (1), 40–50.
- Pavlis, N.K., Holmes, S.A., Kenyon, S.C., Factor, J.K., 2012. The development and evaluation of the Earth Gravitational Model 2008 (EGM2008). *J. Geophys. Res. Solid Earth* 117 (B4), B04406.
- Qiu, B., Chen, S., Klein, P., Wang, J., Torres, H., Fu, L.L., Menemenlis, D., 2018. Seasonality in transition scale from balanced to unbalanced motions in the world ocean. *J. Phys. Oceanogr.* 48 (3), 591–605.
- Raney, R.K., Phalippou, L., 2011. The future of coastal altimetry. In: Vignudelli, Stefano, Kostianoy, Andrey G., Cipollini, Paolo, Benveniste, Jérôme (Eds.), *Coastal Altimetry*. Springer, Berlin, Heidelberg, pp. 535–560.
- Sandwell, D.T., Smith, W.H., 2005. Retracking ers-1 altimeter waveforms for optimal gravity field recovery. *Geophys. J. Int.* 163 (1), 79–89.
- Sandwell, D.T., Smith, W.H., Gille, S., Kappel, E., Jayne, S., Soofi, K., Coakley, B., Géli, L., 2006. Bathymetry from space: Rationale and requirements for a new, high-resolution altimetric mission. *C.R. Geosci.* 338 (14–15), 1049–1062.
- Sandwell, D.T., Smith, W.H., 2009. Global marine gravity from retracked Geosat and ERS-1 altimetry: Ridge segmentation versus spreading rate. *J. Geophys. Res. Solid Earth* 114 (B1), B01411.
- Sandwell, D.T., Müller, R.D., Smith, W.H., Garcia, E., Francis, R., 2014. New global marine gravity model from CryoSat-2 and Jason-1 reveals buried tectonic structure. *Science* 346 (6205), 65–67.
- Smith, W.H.F., 2015. The resolution of seamount geoid anomalies achieved by the SARAL AltiKa and Envisat RA2 satellite radar altimeters. *Mar. Geod.* 38 (Suppl. 1), 664–671.
- Wessel, P., Bercovici, D., 1998. Interpolation with splines in tension: a Green's function approach. *Math. Geol.* 30 (1), 77–93.
- Wessel, P., Smith, W.H., Scharroo, R., Luis, J., Wobbe, F., 2013. Generic mapping tools: improved version released. *Eos, Trans. Am. Geophys. Union* 94 (45), 409–410.
- Zhang, S., Sandwell, D.T., 2017. Retracking of SARAL/AltiKa radar altimetry waveforms for optimal gravity field recovery. *Mar. Geod.* 40 (1), 40–56.
- Zhang, S., Li, J., Jin, T., Che, D., 2018. Hy-2a altimeter data initial assessment and corresponding two-pass waveform retracker. *Remote Sens.* 10 (4), 507.
- Zhang, S., Sandwell, D.T., Jin, T., Li, D., 2017. Inversion of marine gravity anomalies over southeastern China seas from multi-satellite altimeter vertical deflections. *J. Appl. Geophys.* 137, 128–137.
- Zaron, E.D., DeCarvalho, R., 2016. Identification and reduction of retracker-related noise in altimeter-derived sea surface height measurements. *J. Atmos. Oceanic Technol.* 33 (1), 201–210.